Journal of Alloys and Compounds 499 (2010) 166–170

Contents lists available at ScienceDirect

Journal of Alloys and Compounds

journal homepage: www.elsevier.com/locate/jallcom

Inductively coupled plasma-assisted RF magnetron sputtering deposition of boron-doped microcrystalline Si films

S.Y. Huang[a], Q.J. Cheng[b], S. Xu[a,*], K. Ostrikov[b]

[a] Plasma Sources and Applications Centre, NIE, Nanyang Technological University, 1 Nanyang Walk, 637616 Singapore, Singapore
[b] Plasma Nanoscience Centre Australia (PNCA), CSIRO Materials Science and Engineering, P.O. Box 218, Lindfield, NSW 2070, Australia

ARTICLE INFO

Article history:
Received 18 November 2009
Received in revised form 13 January 2010
Accepted 16 January 2010
Available online 25 January 2010

Keywords:
Microcrystalline silicon
Boron doping
Inductively coupled plasmas
Solar cells

ABSTRACT

An innovative custom-designed inductively coupled plasma-assisted RF magnetron sputtering deposition system has been developed to synthesize B-doped microcrystalline silicon thin films using a pure boron sputtering target in a reactive silane and argon gas mixture. Films were deposited using different boron target powers ranging from 0 to 350 W at a substrate temperature of 250 °C. The effect of the boron target power on the structural and electrical properties of the synthesized films was extensively investigated using X-ray diffraction, Raman spectroscopy, scanning electron microscopy, and Hall-effect system. It is shown that, with an initial increase of the boron target power from 0 to 300 W, the structural and electrical properties of the B-doped microcrystalline films are improved. However, when the target power is increased too much (e.g. to 350 W), these properties become slightly worse. The variation of the structural and electrical properties of the synthesized B-doped microcrystalline thin films is related to the incorporation of boron atoms during the crystallization and doping of silicon in the inductively coupled plasma-based process. This work is particularly relevant to the microcrystalline silicon-based *p–i–n* junction solar cells.

1. Introduction

Recently, boron-doped microcrystalline silicon and microcrystalline Si-based alloys have attracted a great deal of attention due to their potential application as a window layer of microcrystalline silicon-based *p–i–n* junction solar cells [1–7]. Compared to B-doped amorphous Si, this material has a higher dark conductivity, carrier mobility, doping efficiency, optical transparency, etc., due to the presence of Si crystallites embedded in the amorphous Si or Si-based matrices [8–14].

In the last decade, various sources of boron such as B_2H_6, $B(CH_3)_3$, and BF_3 have been employed to prepare B-doped microcrystalline Si using a range of deposition techniques including plasma enhanced chemical vapor deposition, hot-wire chemical vapor deposition, photochemical vapor deposition, etc. [1,15–17]. However, to the best of our knowledge, the most commonly used boron sources are toxic. Moreover, the extra elements (such as H element in B_2H_6, C element in $B(CH_3)_3$, and F element in BF_3) in the boron sources may be incorporated into the synthesized films, which may significantly degrade the structural and electrical properties of the B-doped microcrystalline Si films. We are not aware of any reports using a solid source for the growth of B-doped microcrystalline Si films. In this work, a new and innovative approach based on the advanced custom-designed inductively coupled plasma (ICP)-assisted RF magnetron sputtering deposition system has been proposed to synthesize B-doped microcrystalline Si films. By using this approach, it becomes possible to use a solid source of boron atoms (solid boron target) to dope microcrystalline silicon.

2. Experimental details

A custom-designed and innovative low-frequency (460 kHz) ICP-assisted RF magnetron sputtering deposition system, an essential component of the Integrated Plasma-Aided Nanofabrication Facility, has been developed to synthesize B-doped microcrystalline silicon thin films using a pure boron magnetron sputtering target in a reactive silane and argon gas mixture [18,19]. Fig. 1 shows a schematic diagram of the ICP-assisted RF magnetron sputtering deposition system used in this work. In this custom-designed system, it is possible to use the solid boron element as a doping source. An additional benefit is the possibility to control the plasma production and the magnetron sputtering independently through adjusting the RF inductive power and the RF magnetron power, respectively [20]. In the experiments carried out here, the RF inductive power for the plasma production was maintained at 1600 W (the plasma reactor has a diameter of 45 cm and a height of 30 cm, and thus the RF power density has a low value of 33.3 mW/cm^3 [9]) while the variable RF magnetron power (P_{magn}) ranging from 0 to 350 W was applied to the boron target. A low-pressure mixture of SiH_4 and Ar gases with flow rates of 15 and 5 sccm (sccm denotes cubic centimeters per minute at standard temperature and pressure), respectively, was let into the chamber, pre-evacuated to a base pressure of $\sim 10^{-5}$ Pa through the use of a combination of rotary and turbo-molecular pumps. The

* Corresponding author. Tel.: +65 67903818; fax: +65 67903919.
E-mail address: shuyan.xu@nie.edu.sg (S. Xu).

0925-8388/$ – see front matter © 2010 Published by Elsevier B.V.
doi:10.1016/j.jallcom.2010.01.078

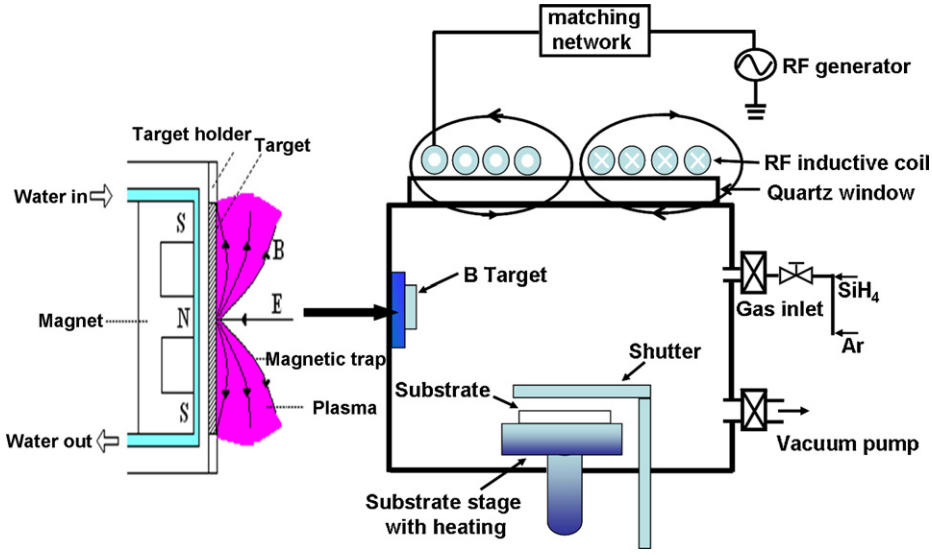

Fig. 1. A schematic diagram of the inductively coupled plasma-assisted RF magnetron sputtering deposition system.

substrate temperature, working gas pressure, and deposition time were fixed at 250 °C, 2.0 Pa, and 30 min, respectively.

The samples were deposited on glass substrates for X-ray diffraction (XRD), Raman scattering, scanning electron microscopy (SEM), and Hall-effect system measurements. The crystalline structure of the synthesized films was investigated using a Siemens D5005 X-ray diffractometer, operated in a locked-couple (θ–2θ) mode, wherein the incident X-ray wavelength was 1.54 Å (Cu Kα line) at 40 kV and 40 mA. Raman measurements were undertaken by a Renishaw 1000 micro-Raman system using a 514.5 nm Ar^+ laser for excitation. The surface morphology and fracture cross-section of the deposited films were investigated using a JEOL JSM-6700F field emission scanning electron microscope fitted with a 30 kV electron gun. The sheet resistance and carrier concentration were obtained by the van der Pauw method using the Hall-effect measurement system (HL5500PC) at room temperature. Samples were cut into squares of dimensions ~10 mm × 10 mm with Al electrodes of four 1-mm radius quarter circle placed at each corner for Ohmic contact.

3. Results

The crystal structure of the synthesized B-doped microcrystalline Si thin films was analyzed by XRD. Fig. 2(a) presents the XRD spectra of the samples deposited at different boron target powers from 0 to 350 W. At a boron target power of 0 W (without turning on the RF magnetron power system), the three main diffraction peaks, located at $2\theta = 28.4^\circ$, 47.3°, and 56.1°, are attributed to the (1 1 1), (2 2 0), and (3 1 1) crystal planes of silicon, respectively [9,21]. One can observe that, without turning on the RF magnetron power system, the intensity of the (1 1 1) peak is much higher than the intensities of the (2 2 0) and (3 1 1) peaks, suggesting that the pure silicon film has a preferential growth along the (1 1 1) crystallographic direction. This preferential growth along the (1 1 1) direction originates from the fact that the (1 1 1) crystal plane is the closest packed Si plane and has the lowest surface energy amongst the all Si crystal planes [9,20]. However, when the power is supplied to the boron target, the preferential crystallographic growth direction changes from (1 1 1) to (2 2 0), as shown in Fig. 2(a). The change of the preferential crystallographic growth direction from (1 1 1) to (2 2 0) is presumably attributed to the combined effects of the surface energy, B-induced nucleation, lateral growth and etching [22,23]. It is noteworthy that this change of the preferential crystallographic growth direction from (1 1 1) to (2 2 0) is particularly useful for the improvement of microcrystalline Si-based solar cell performance. Indeed, in comparison with other crystal orientations, the (2 2 0)-oriented Si films feature electrically inactive (2 2 0)-tilt boundary and compact columnar structures, which is particularly useful for light trapping and carrier transport [22,23].

In order to thoroughly investigate the trend in the variation of the (1 1 1) and (2 2 0) crystallographic directions with the increase of RF magnetron power P_{magn} from 0 to 350 W, we have plotted the integrated XRD intensity ratio of the (2 2 0) to (1 1 1) peaks (designated as $I_{(220)}/I_{(111)}$) as a function of the boron target power in Fig. 2(b). One can observe that $I_{(220)}/I_{(111)}$ initially increases from 0.46 at $P_{magn} = 0$ to 26.5 W (maximum value) at a boron target power of 300 W, and then is slightly reduced when the boron target power is further increased, reaching a value of 12.8 at $P_{magn} = 350$ W. The slight decrease of $I_{(220)}/I_{(111)}$ with the increased magnetron sputtering power from 300 to 350 W suggests that the

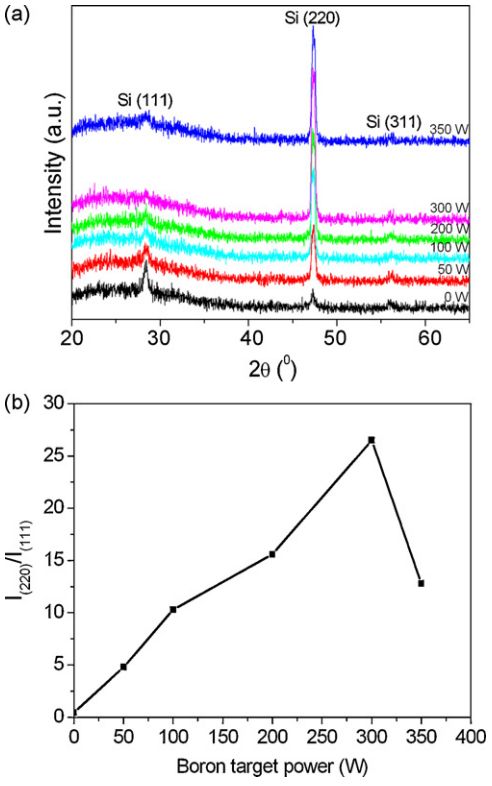

Fig. 2. (a) XRD spectra of the samples deposited at different boron target powers from 0 to 350 W. (b) The integrated XRD intensity ratio of the (2 2 0) to (1 1 1) peaks (designated as $I_{(220)}/I_{(111)}$) as a function of the boron target power.

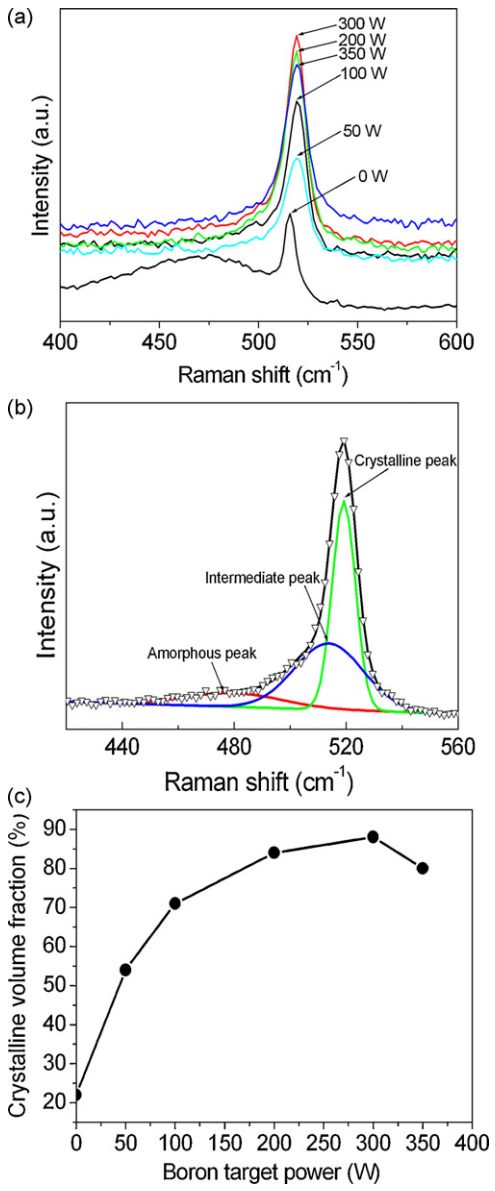

Fig. 3. (a) Raman scattering spectra of the samples deposited at different boron target powers. (b) A typical deconvolution of the Raman spectrum of the sample deposited at a boron target power of 300 W. (c) The estimated crystalline volume fraction X_C as a function of the boron target power.

crystallinity degree of the synthesized B-doped microcrystalline silicon films is diminished above a certain value of the boron target power. This is confirmed by Raman measurements below.

The crystallinity of the deposited films was further studied by Raman spectroscopy. Fig. 3(a) represents the Raman scattering spectra of the samples deposited at different boron target powers. The dominant peak in all the spectra is located at approximately 520 cm^{-1} and is attributed to the transverse optical mode of crystalline Si, indicating that all the deposited films are in the state of crystalline phase [24].

For detailed study of the variation of the degree of crystallinity of the deposited films, we have deconvoluted the dominant Raman peak into three independent Gaussian peaks: a crystalline silicon narrow peak near 520 cm^{-1}, an intermediate peak near 500–510 cm^{-1} (attributed to small crystallites or grain boundaries), and a broad peak centered at 480 cm^{-1} (characteristic of the amorphous silicon phase) [23,25]. Fig. 3(b) displays a typical deconvolution of the Raman spectrum of the sample deposited at P_{magn} = 300 W. The crystalline volume fraction X_C can be deduced from the deconvoluted spectra through the sum of the integrated intensities of the individual crystalline and intermediate Si peaks divided by the total sum of the integrated intensities of the individual crystalline, intermediate, and amorphous peaks.

Fig. 3(c) shows the estimated crystalline volume fraction X_C, deduced from the deconvoluted spectra, as a function of the boron target power. Without applying any RF magnetron power to the boron target, X_C has a low value of 22%. However, when a low RF power is applied to the boron target (P_{magn} = 50 W), X_C rapidly increases to 54%. Then, X_C keeps increasing until a boron target power of 300 W is reached. With a further increase of P_{magn} from 300 to 350 W, X_C displays a slight reduction from 88% at P_{magn} = 300 W to 80% when the boron target power reaches 350 W.

The morphological and microstructural properties of the deposited films were studied by SEM. Fig. 4(a and b) presents the typical surface morphological and cross-sectional images of the sample deposited at a boron target power of 300 W. As shown in Fig. 4(a), the B-doped microcrystalline film has a clearly faceted morphology with a hexagonal shape. With careful examination, one can observe that the microstructure contains ultra-small nanoparticles with sizes of a few nanometers. The cross-sectional imaging shown in Fig. 4(b) reveals that the deposited film develops as a vertically aligned columnar structure with clear boundaries between the individual columnar grains. This columnar structure is beneficial for effective light trapping and carrier transport in Si-based thin-film solar cell applications [9].

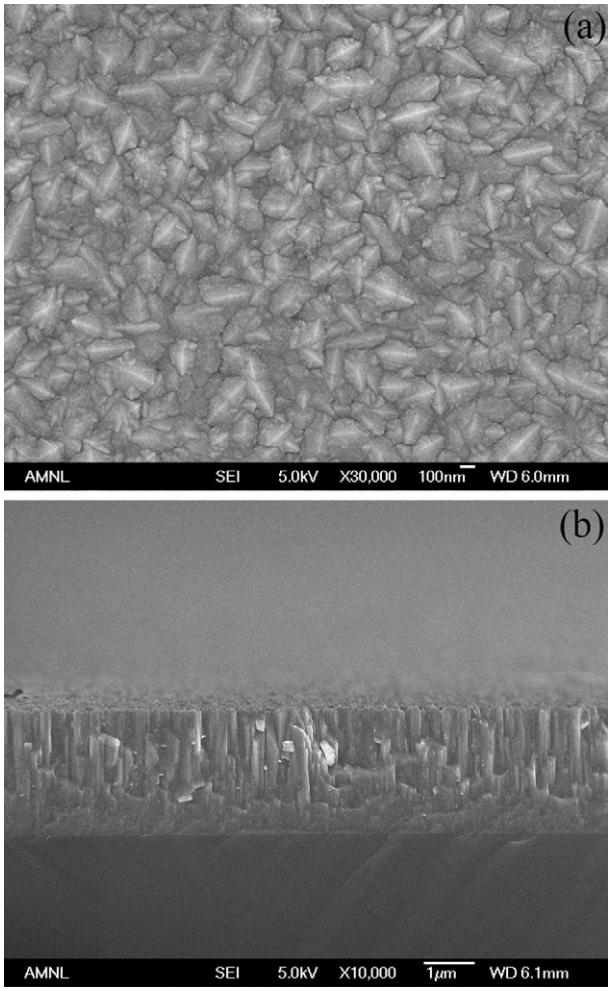

Fig. 4. (a and b) The typical surface morphological (a) and cross-sectional (b) images of the sample deposited at a boron target power of 300 W.

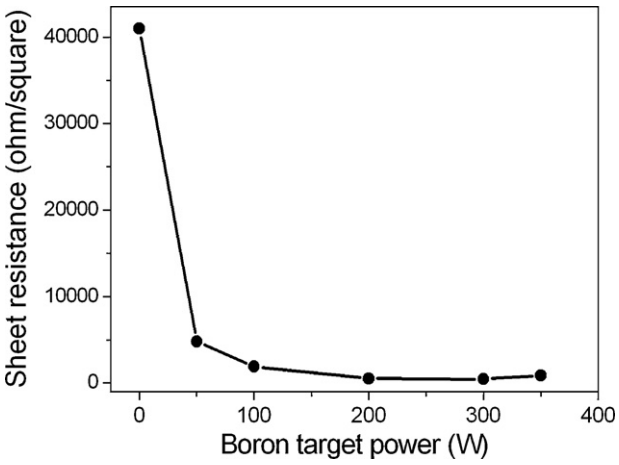

Fig. 5. Variation of the sheet resistance with the boron target power.

The electrical properties of the deposited films were investigated using the Hall-effect system. The variation of the sheet resistance with the boron target power is presented in Fig. 5. Initially, the sheet resistance decreases markedly by one order of magnitude from 4.1×10^4 to 4.8×10^3 ohm/square with the increase of the boron target power from 0 to 50 W. However, with a further increase of the boron target power until 300 W, although the sheet resistance keeps decreasing, it does not vary significantly, reaching the lowest value of 456 ohm/square at a boron target power of 300 W. With a further increase of P_{magn} from 300 to 350 W, the sheet resistance increases slightly from 456 to 865 ohm/square. It is worthwhile to mention that the variation of the carrier concentration shows a reverse trend to the sheet resistance when the boron target power is increased. With the increased P_{magn} from 0 to 300 W, the carrier concentration 5×10^{16} cm^{-3} at P_{magn} = 0 W to a maximum value of 4.8×10^{19} cm^{-3} at P_{magn} = 300 W. However, with a further increase of P_{magn} from 300 to 350 W, the carrier concentration decreases slightly from 4.8×10^{19} cm^{-3} to 4.1×10^{19} cm^{-3}.

4. Discussion

XRD, Raman, and sheet resistance analyses reveal that, with an initial increase of the boron target power from 0 to 300 W, the structural and electrical properties of the deposited B-doped microcrystalline films are improved. The highest crystalline volume fraction of 88%, the lowest sheet resistance of 456 ohm/square, and the highest carrier concentration of 4.8×10^{19} cm^{-3} are obtained at a boron target power of 300 W. However, when the target power is increased too much (e.g. 350 W), the structural and electrical properties of the synthesized films become slightly worse. These experimental results are related to the incorporation of boron atoms into the Si lattice during the crystallization of silicon in the inductively coupled plasma-based doping process [26].

In comparison with an RF capacitive discharge where RF power is coupled into the plasma by electrostatic coupling, the power is transferred across a dielectric window via electromagnetic coupling in ICP discharges operated in the electromagnetic mode. This non-capacitive power transfer is effective in reducing plasma sheath potentials at wall surfaces, electrodes and substrates, and therefore diminishes the bombarding energy of the ions impinging on the growth surface [18,27,28]. It also provides an independent control of the ion/radical fluxes and ion-bombarding energy. Moreover, the inductively coupled plasma source features high-densities of electrons and ions. The typical plasma density achieved in the ICP discharge is about a factor of 10–100 times higher than those produced by capacitive discharges under quite similar conditions [18,27,28]. As such, ICP-enhanced chemical vapor deposition has attracted a great deal of interest for low-pressure, low-temperature material processing [9,18,29,30]. In particular, by using an external source of high-density ICPs, one can dramatically increase the sputtering yield from solid targets in magnetron sputtering deposition systems [18–20,31,32]. This is because the plasmas can significantly enhance the dissociation and ionization of carrier gases via strong electron impact reactions, which in turn leads to much larger ion fluxes impinging on the sputtering surface [18–20,31–33].

We stress that the crystallization process of microcrystalline Si in the ICP-based process is quite different from the standard (13.56 MHz) capacitively coupled RF plasma-based process. In the capacitively coupled RF plasma-based process, the high RF power and heavy hydrogen dilution are routinely used to enable the crystallization of silicon [8,15]. This is because, under such conditions, a large coverage factor of hydrogen on the growing surface can be achieved, which facilitates the crystallization of silicon through the reduction of the surface reactivity of the Si-based radicals and the associated surface diffusion activation barriers [30,34,35]. However, this process frequently significantly degrades the film quality because of the formation of powder particles and the heavy ion bombardment of the growth surface [35–37]. In contrast, in the ICP-based process, heavy hydrogen dilution and/or high RF power are not essential for Si crystallization because of the outstanding dissociation ability of the high-density inductively coupled plasmas. Thereby, the large coverage factor of hydrogen on the growth surface, a prerequisite for the crystallization of Si, can be delivered via the highly effective dissociation of silane precursor in the ICP-based process even without any hydrogen dilution. A detailed study of the crystallization process of the undoped (intrinsic) silicon in the ICP-based process has been presented in our previous works [9,23,30,38].

5. Conclusions

In summary, a custom-designed ICP-assisted RF magnetron sputtering system has been proposed to synthesize B-doped microcrystalline silicon films from the silane and argon precursor gases without any additional hydrogen dilution at a substrate temperature of 250 °C. A broad range of advanced characterization tools have been used to study the structural and electrical properties of the synthesized films when the input boron target power is varied from 0 to 350 W. In particular, at a boron target power of 300 W, the film features the highest crystalline volume fraction of 88%, the lowest sheet resistance of 456 ohm/square, the highest carrier concentration of 4.8×10^{19} cm^{-3}, and also exhibits a preferential growth along the (2 2 0) crystallographic direction. The SEM cross-sectional analysis also reveals a vertically aligned columnar structure. The obtained experimental results have been interpreted in terms of the effects of substitutional boron atoms on the crystallization and doping processes of silicon in the high-density inductively coupled plasma-based process.

Acknowledgements

This work was partially supported by the National Research Foundation (Singapore), CSIRO, and the Australian Research Council (Australia). We thank A.E. Rider for valuable comments and proofreading of the revised manuscript.

References

[1] T. Toyama, W. Yoshida, Y. Sobajima, H. Okamoto, J. Non-Cryst. Solids 354 (2008) 2204.
[2] A. Merabet, J. Alloys Compd. 382 (2004) 300.
[3] Z. Li, W. Zhou, T. Lei, F. Luo, Y. Huang, Q. Cao, J. Alloys Compd. 475 (2009) 506.

[4] B.P. Swain, B.S. Swain, S.H. Park, N.M. Hwang, J. Alloys Compd. 480 (2009) 878.
[5] N.M. Hwang, D.Y. Kim, Int. Mater. Rev. 49 (2004) 171.
[6] X. Liu, Y. Wu, X. Bian, J. Alloys Compd. 391 (2005) 90.
[7] A. Haarahiltunen, H. Talvitie, H. Savin, M.Y. Koski, M.I. Asghar, J. Sinkkonen, Appl. Phys. Lett. 92 (2008) 021902.
[8] R. Saleh, N.H. Nickel, Thin Solid Films 427 (2003) 266.
[9] Q.J. Cheng, S. Xu, S.Y. Huang, K. Ostrikov, Cryst. Growth Des. 9 (2009) 2863.
[10] J.B. Misiuk, A. Misiuk, A. Shalimov, V.G. Zavodinsky, A.A. Gnidenko, B. Surma, et al., J. Alloys Compd. 382 (2004) 160.
[11] I.B. Denysenko, K. Ostrikov, S. Xu, M.Y. Yu, C.H. Diong, J. Appl. Phys. 94 (2003) 6097.
[12] L.S. Chuah, Z. Hassan, S.S. Ng, H.A. Hassan, J. Alloys Compd. 479 (2009) L54.
[13] W.A. Badawy, J. Alloys Compd. 464 (2008) 347.
[14] J.L. Zhang, J. Li, L.M. Luo, Y.H. Wo, J. Alloys Compd. 469 (2009) 535.
[15] T. Matsui, M. Kondo, A. Matsuda, J. Non-Cryst. Solids 338–340 (2004) 646.
[16] P. Kumar, M. Kupich, D. Grunsky, B. Schroeder, Thin Solid Films 501 (2006) 260.
[17] J. Kwak, S.W. Kwon, S.I. Park, J.H. Yang, K.S. Lim, Sol. Energy Mater. Sol. Cells 92 (2008) 1081.
[18] S. Xu, K. Ostrikov, J.D. Long, S.Y. Huang, Vacuum 80 (2006) 621.
[19] Q.J. Cheng, S. Xu, J.D. Long, K. Ostrikov, Appl. Phys. Lett. 90 (2007) 173112.
[20] B.S. Chua, S. Xu, Y.P. Ren, Q.J. Cheng, K. Ostrikov, J. Alloys Compd. 485 (2009) 379.
[21] M. Jeon, K. Kamisako, J. Alloys Compd. 476 (2009) 84.
[22] C. Das, A. Dasgupta, S.C. Saha, S. Ray, J. Appl. Phys. 91 (2002) 9401.
[23] Q.J. Cheng, S. Xu, K. Ostrikov, J. Phys. Chem. C 113 (2009) 14759.
[24] M. Xu, S. Xu, J.W. Chai, J.D. Long, Y.C. Ee, Appl. Phys. Lett. 89 (2006) 251904.
[25] J. Wang, P. Gao, M. Yin, Y. Qin, H. Yan, J. Li, S. Peng, D. He, J. Alloys Compd. 481 (2009) 278.
[26] P.E. Vanier, J. Tafto, G. Rajeswaran, F.J. Kampas, J. Non-Cryst. Solids 66 (1984) 31.
[27] I.B. Denysenko, S. Xu, J.D. Long, P.P. Rutkevych, N.A. Azarenkov, K. Ostrikov, J. Appl. Phys. 95 (2004) 2713.
[28] K.N. Ostrikov, S. Xu, A.B.M.S. Azam, J. Vac. Sci. Technol. A 20 (2002) 251.
[29] U. Cvelbar, M. Mozetic, M.K. Sunkara, S. Vaddiraju, Adv. Mater. 17 (2005) 2138.
[30] Q.J. Cheng, S. Xu, K. Ostrikov, J. Mater. Chem. 19 (2009) 5134.
[31] S.Y. Huang, K. Ostrikov, S. Xu, J. Appl. Phys. 104 (2008) 033301.
[32] Q.J. Cheng, J.D. Long, S. Xu, J. Appl. Phys. 101 (2007) 094304.
[33] U. Cvelbar, Z. Chen, M.K. Sunkara, M. Mozetič, Small 4 (2008) 1610.
[34] K. Ostrikov, Rev. Mod. Phys. 77 (2005) 489.
[35] K.N. Ostrikov, M.Y. Yu, L. Stenflo, Phys. Rev. E 61 (2000) 782.
[36] K. Ostrikov, A.B. Murphy, J. Phys. D: Appl. Phys. 40 (2007) 2223.
[37] P.P. Rutkevych, K. Ostrikov, S. Xu, S.V. Vladimirov, J. Appl. Phys. 96 (2004) 4421.
[38] Q.J. Cheng, S. Xu, K. Ostrikov, Nanotechnology 20 (2009) 215606.